Front. Archit. Civ. Eng. China 2011, 5(2): 208–224
DOI 10.1007/s11709-011-0111-0

RESEARCH ARTICLE

Hehua ZHU, Qianwei XU, Wenqi DING, Feng HUANG

Experimental study on the progressive failure and its anchoring effect of weak-broken rock vertical slope

Abstract To improve the understanding on the failure behavior and its anchoring effect of weak-broken rock slope, the rock of grade IV according to China is taken as reference prototype, and a series of model tests were carried out in laboratory. These tests can be divided into two categories, that is, with bolt reinforcement and without bolt reinforcement. In which, the stability of slope reinforced with different bolt diameter, different anchor length and different space are studied. The test results show that the collapse of slope is the combination of tension failure at the top and the compression-shearing failure at the bottom of the slope, and its failure process presents progressive characteristics. The contributions of bolt reinforcement are mainly reflected by the aspects of shear resistance, crack resistance and anti-extension. The reinforcement of blot not only can improve the vertical bearing capacity before failure, but also can reduce the vertical settlement and allow greater lateral rock wall deformation; what is more, the stress concentration degree in rock mass can be dispersed, which do help to improve the stability of slope rock mass.

Keywords progressive failure, weak-broken rock, slope, model test, bolt

1 Introduction

With the rapid development of highway and railway construction in China, there are more and more cases of cutting slope to construct the roadbed or excavating tunnel in unfavorable geological condition or special geological area. Therefore, a large number of high rock slopes will be generated. As proven by engineering practices and field investigations, the activities of cutting slope and excavating tunnel will not only disturb the original balance state but also lead to stress redistribution in rock mass, especially for the natural rock mass widely distributed with all kinds of weak structural planes. In such circumstance, the surrounding rock will be damaged due to high stress concentration or excessive deformation. In most cases, the failure mode of the weak-broken rock mass seldom enters into overall instability state directly, but always starts form slow steady-state with uniform deformation and then enters into progressive failure mode with intense localization deformation [1]. At present, the studies on localization progressive failure of rock mass are mainly conducted by means of theoretical analysis, numerical simulation and in situ monitoring [2–11]. However, due to the complexity of this problem, theoretical researches have developed slowly in recent years. In addition, it is also impossible to carry out a large number of field measurements for the sake of test site constraints and shortage of funds. Therefore, laboratory model tests have played an important role in the studies on the failure process of weak-broken rock slope. For example, Yuan et al. [12] simulated the load-off process of high rock slope excavation through a 3-dimensional model experiment. Wu et al. [13] carried out an indoor model test on cracked rock mass reinforced by bolt, and the deformation and strength character of the rock was studied. Chen et al. [14] conducted the research on simulating the progressive failure law of jointed rock slope in consideration of only gravity function with self-designed base friction tester. Liu et al. [15] studied the failure problems of open pit slope through numerical simulation and similar model test. In summary, some achievements on progressive failure characteristics and stability analysis of weak-broken rock slope have been made in recent years;

Received March 15, 2011; accepted April 10, 2011

Hehua ZHU (✉), Qianwei XU, Wenqi DING, Feng HUANG
Key Laboratory of Geotechnical and Underground Engineering of Ministry of Education, Tongji University, Shanghai 200092, China
E-mail: zhuhehua@tongji.edu.cn

Qianwei XU
Urban Rail Transit and Railway Engineering Department, Tongji University, Shanghai 200092, China

however, due to the complexity of geotechnical engineering, it is still necessary to carry out further research on this problem.

In this paper, a series of model tests were carried out to study the failure behavior of weak-broken vertical rock slope and it anchoring effect. The test results cannot only provide reference for the design and construction of slope engineering, but also help to improve the self-stabilizing ability of engineering rock mass.

2 Principles of model test

As an extreme slope form, the vertical rock slope is selected as research object in our model tests. Due to the restraint of test condition, it is impossible to manufacture each indoor slope model with different excavated height. Therefore, only one type model was manufactured, and its surface was applied with different uniform distributed overburden loads. As shown in Fig. 1, in order to simulate the excavation of slope, a special metal box with dimension of 400mm × 300mm × 300mm was manufactured. Its four side faces are all fixed except that the top side is open. Among them, the front area 1 was installed with plexiglass for observing the deformation of rock mass, area 2 can be removed to simulate vertical slope after excavation. The inner walls of the box were coated with a layer of grease to reduce the friction between wall and model ground.

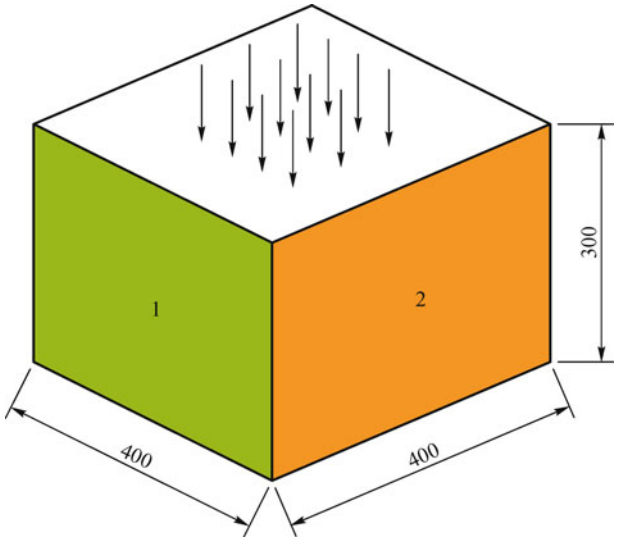

Fig. 1 Sketch map of loading in model test (unit: mm)

3 Similarity principles and model materials

Similar model test is an effect way in analyzing and solving prototype engineering problems according to the similitude theory by observing the model behaviors of displacement, deformation and destruction. As for rock material, it belongs to the scope of geomechanical model test. Therefore, the model geometry dimension, boundary conditions, applied loads, material density, mechanical strength and deformation characteristics, etc., are all required to satisfy the similar requirements expressed by Eqs. (1)–(5).

$$C_\sigma = C_l C_\gamma, \tag{1}$$

$$C_\sigma = C_E C_\varepsilon, \tag{2}$$

$$C_\mu = 1, \tag{3}$$

$$C_\delta = C_l C_\varepsilon, \tag{4}$$

$$C_{\overline{\sigma}} = C_\sigma, \tag{5}$$

where, C is the similar proportion, σ is stress, l is geometry dimension, γ is bulk density, E is elastic modulus, ε is strain, μ is poison ratio, δ is deformation and $\overline{\sigma}$ is area load.

According to above relationships, once the geometry similarity ratio is selected, the suitable model materials should be found to satisfy the requirements of mechanical strength and deformation. In our tests, the reference prototype rock is grade IV according to China classification. Its corresponding mechanical properties can be found in the code for design of road tunnel of China, as shown in Table 1.

The similarity ratios used in the model test are shown as below:

geometry similarity ratio $C_l = 50$, bulk density similarity ratio $C_\gamma = 1$, poison similarity ratio $C_\mu = 1$, strain similarity ratio $C_\varepsilon = 1$, friction angle similarity ratio $C_\varphi = 1$, stress similarity ratio $C_\sigma = 50$, elastic modulus similarity ratio $C_E = 50$.

The model ground should be prepared according to above similarity ratio. The selected experimental material is a mixture of barite, sand, plaster and water in a weight ratio of 12:4:2:1.5. For meeting the required mechanical strength, the material should be compacted to the certain density first, and then placed 3 days before testing. Its mechanical properties are shown in Table 1.

As for the bolt, its similarity requirement is mainly

Table 1 Prototype and model rock mechanical properties

grade IV rock	bulk density /(kN·m^{-3})	elastic modulus/GPa	poison ratio	cohesion force/MPa	friction angle/(°)
prototype	20~23	1.3~6.0	0.3~0.35	0.2~0.7	27~39
model	20~23	0.026~0.120	0.30~0.35	0.004~0.014	27~39

reflected by the linear stiffness and the amount of steel in unit area of tunnel wall. The similarity of linear stiffness is shown in following formula:

$$C_{EA} = \frac{(EA)_{\mathrm{p}}}{(EA)_{\mathrm{m}}} = C_E C_L^2, \tag{6}$$

where EA is the bolt linear stiffness, the subscripts of p and m represent the prototype and the model respectively.

According to above similarity criteria, different copper tubes with diameter of 1.5, 1.8 and 2.0 mm are selected as model bolts.

4 Design of model test

4.1 Displacement measurement

As shown in Figs. 2 and 3, the C050 displacement meter is arranged 5 cm away from the side area 2 to measure ground surface displacement; the other two meters, C051 and C052, arranged 10 cm and 20 cm away from the bottom respectively are used to measure the lateral displacement of side area 2.

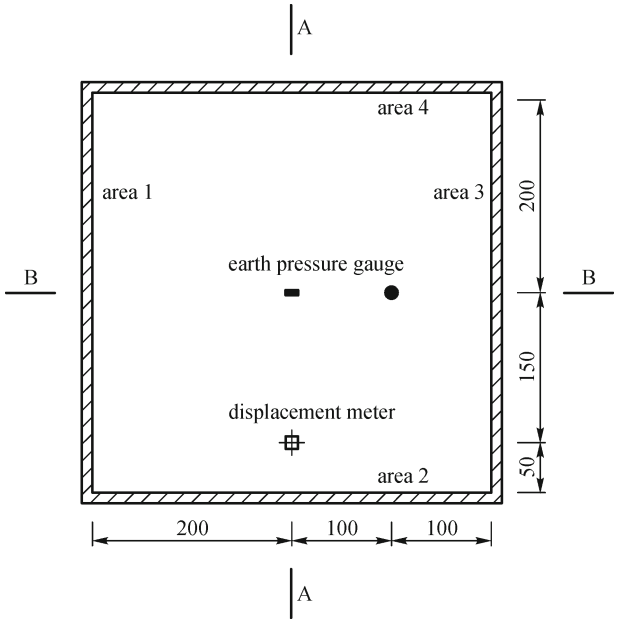

Fig. 2 Measure layout of displacement and stress (unit: mm)

4.2 Stress measurement

As shown in Figs. 2 and 4, in order to measure the variation of stress inside rock mass during the excavation of vertical slope, 10 earth pressure gauges are embedded at different position. Among them, the five gauges, C040, C042, C044, C046 and C048 are used to measure the horizontal stress; the other five gauges, C041, C043, C045, C047 and C049 are used to measure vertical stress.

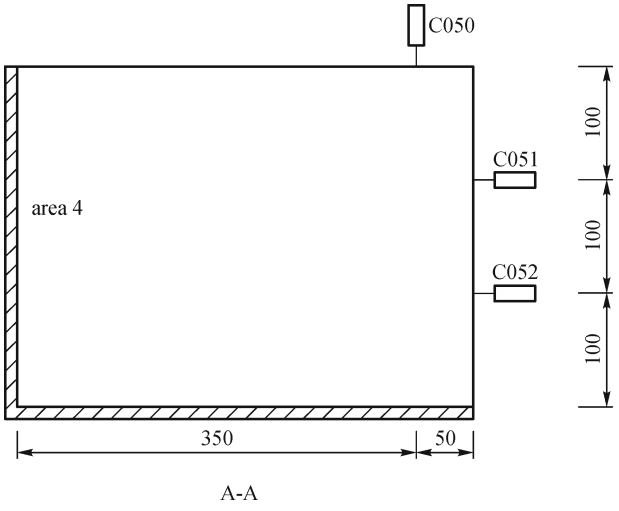

Fig. 3 Elevation view of displacement measurement (unit: mm)

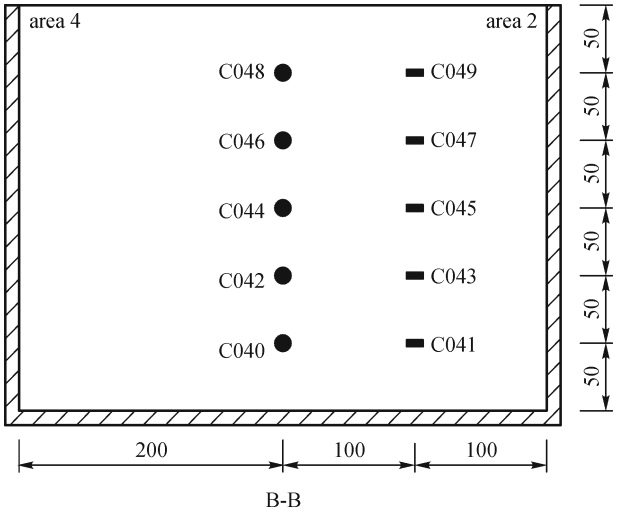

Fig. 4 Elevation view of stress measurement (unit: mm)

4.3 Design of test cases

The tests are mainly divided into two categories, namely, no bolt support and bolt support. Case 1 is conducted without bolt support. As shown in Figs. 5 to 10, bolts are arranged with different diameter, different length and different space in case 2 to case 7.

5 Analysis of test results

5.1 Failure process analysis

To study the failure mode of vertical rock slope, uniform pressure was applied on the model ground surface step by step.

Case 1: In this test, there was no bolt reinforced. As shown in Fig. 11, with the increase of upper load, the

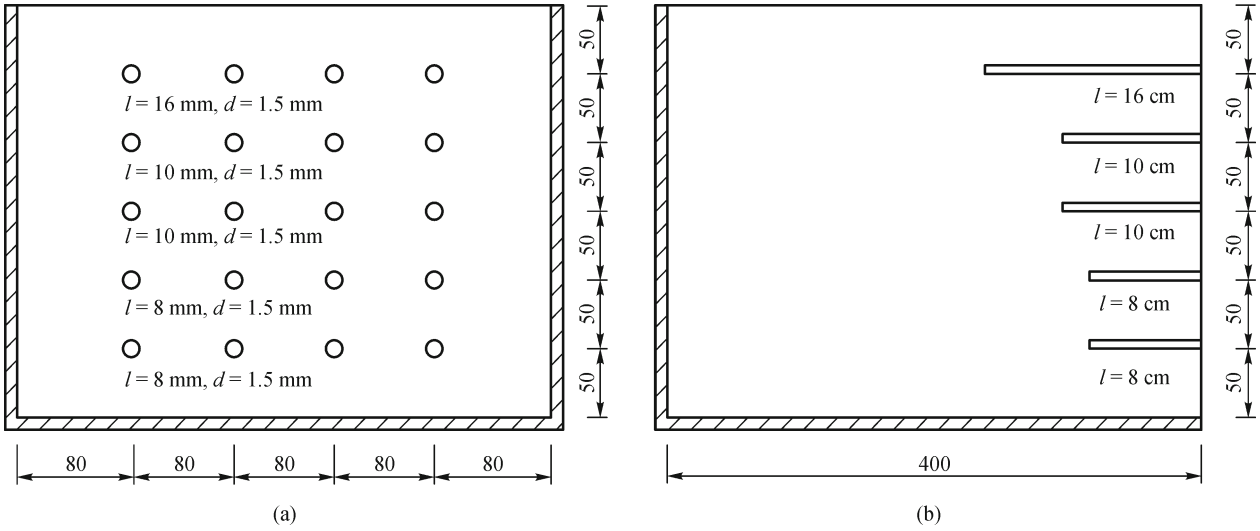

Fig. 5 Arrangement of bolt. (a) Elevation view of bolt arrangement; (b) profile of bolt arrangement (case 2, unit: mm)

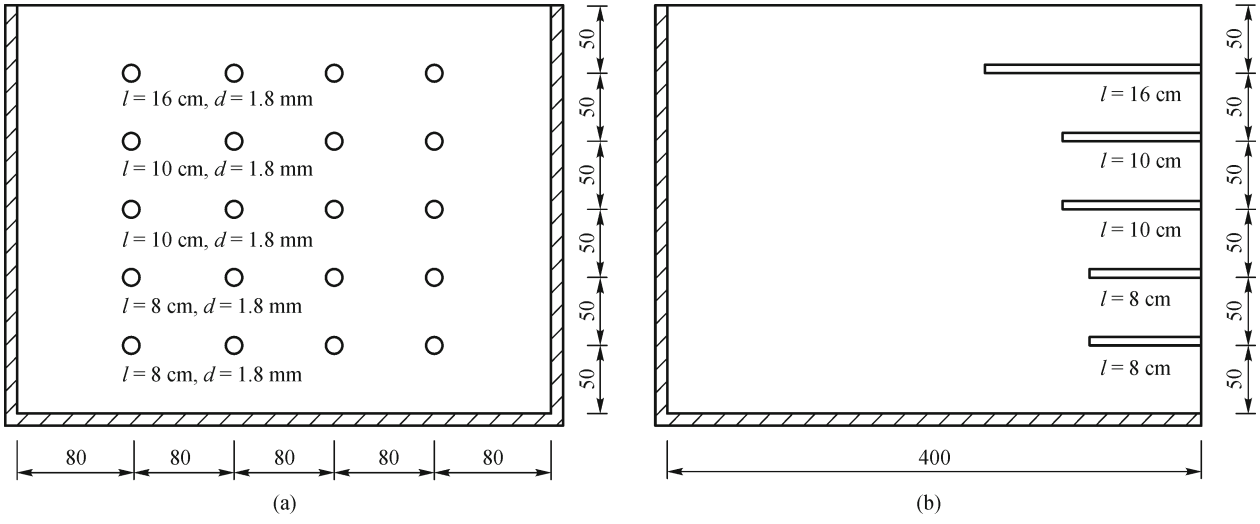

Fig. 6 Arrangement of bolt. (a) Elevation view of bolt arrangement; (b) profile of bolt arrangement (case 3, unit: mm)

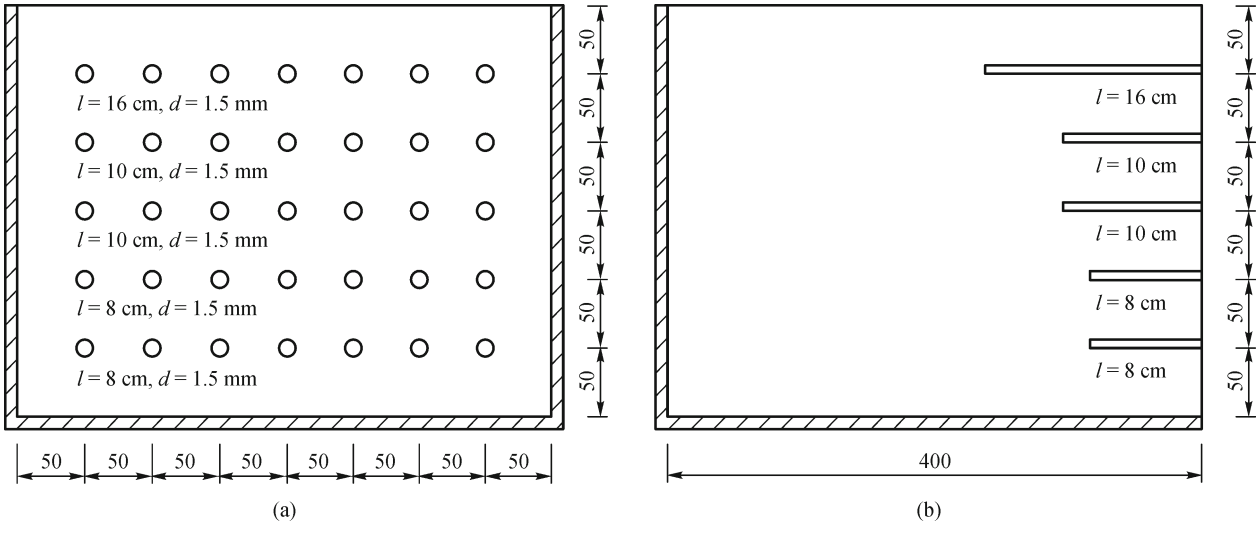

Fig. 7 Arrangement of bolt. (a) Elevation view of bolt arrangement; (b) profile of bolt arrangement (case 4, unit: mm)

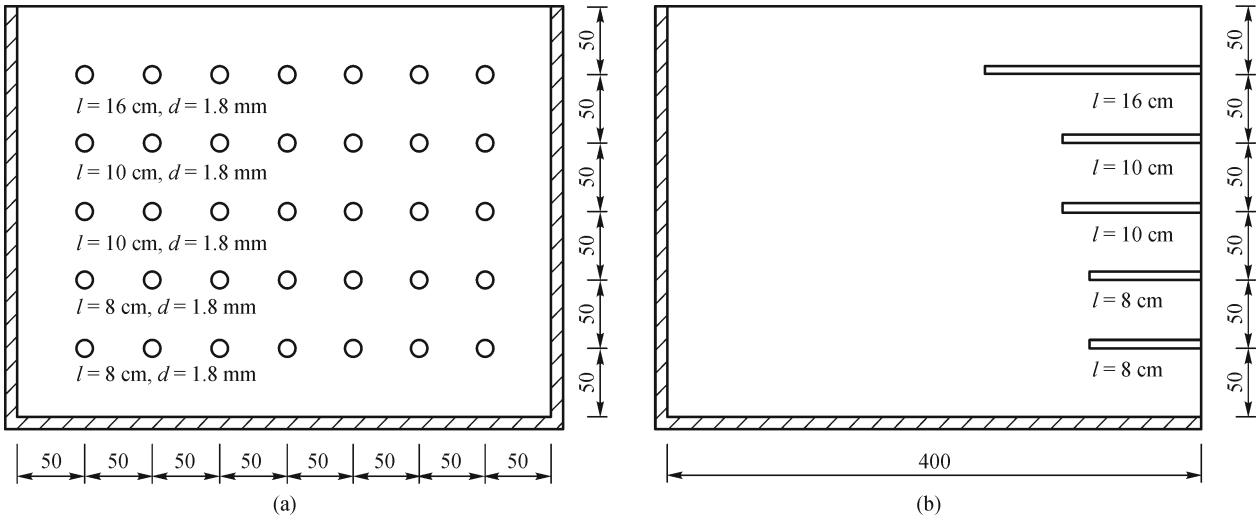

Fig. 8 Arrangement of bolt. (a) Elevation view of bolt arrangement; (b) profile of bolt arrangement (case 5, unit: mm)

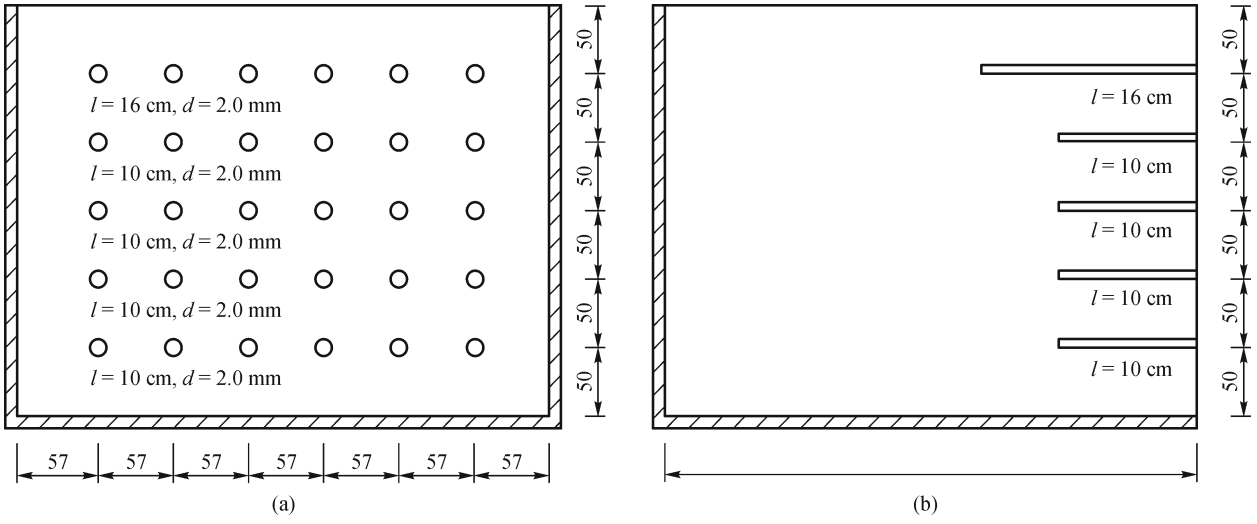

Fig. 9 Arrangement of bolt. (a) Elevation view of bolt arrangement; (b) profile of bolt arrangement (case 6, unit: mm)

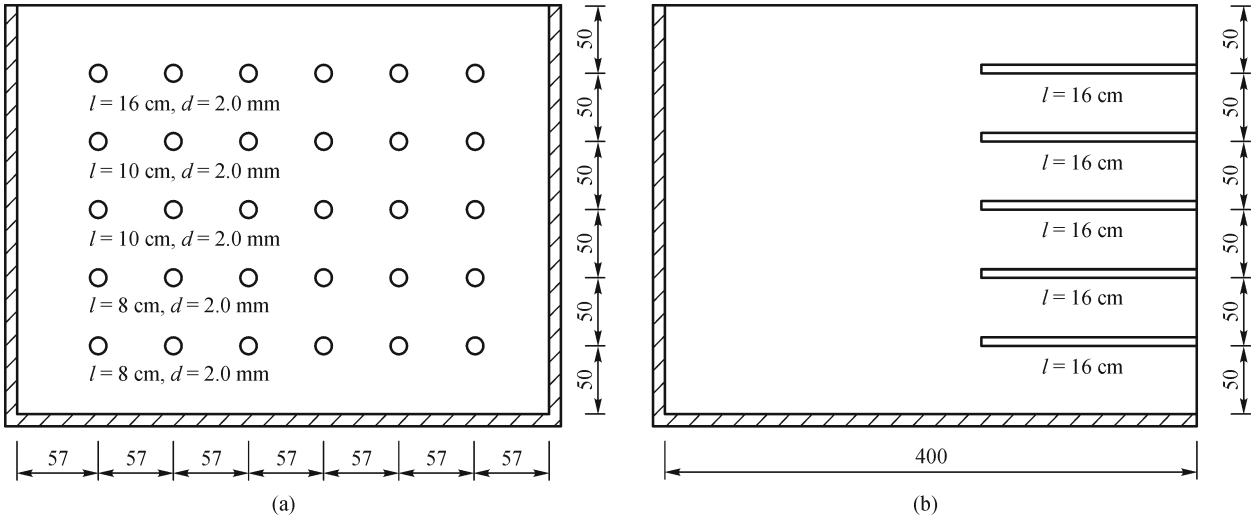

Fig. 10 Arrangement of bolt. (a) Elevation view of bolt arrangement; (b) profile of bolt arrangement (case 7, unit: mm)

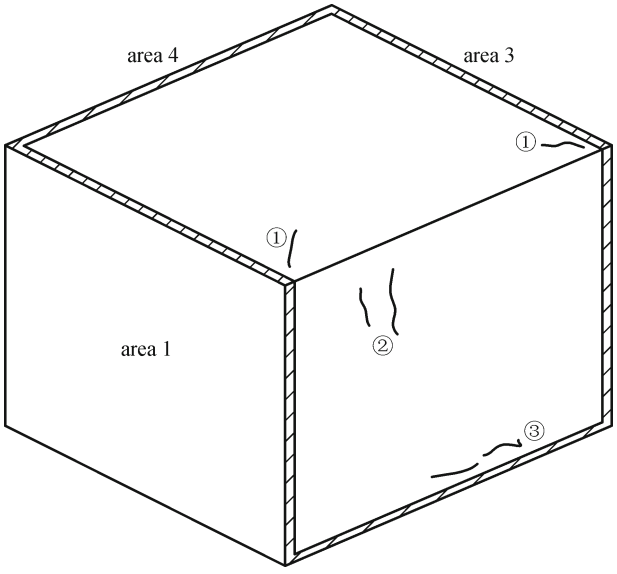

Fig. 11 Progressive failure process of the vertical slope without bolt reinforcement in case 1

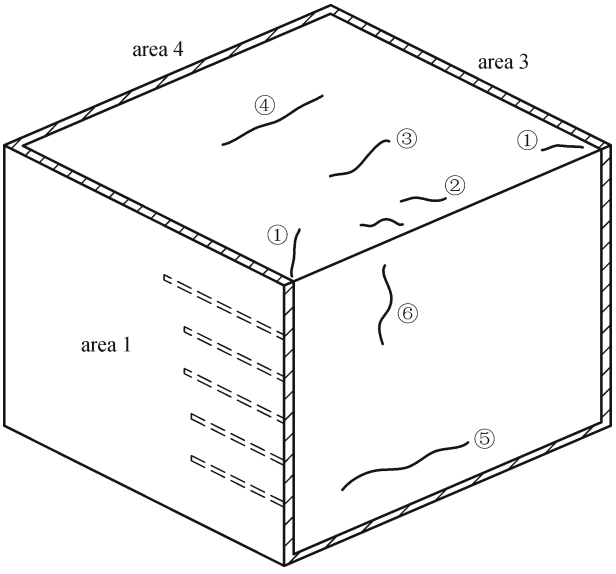

Fig. 13 Progressive failure process of the vertical slope with bolt reinforcement in case 2

oblique cracks ① were first appeared at the intersection of ground surface and side area 2. Subsequently, the vertical cracks ② were appeared at the top of vertical area 2 and short horizontal cracks ③ near the bottom. When the load increased to 848N, the failure started from the bottom of side area 2, then quickly extended upwards to the ground surface and formed the final sliding face ④. As shown in Fig. 12, the final sliding face was in approximated arc-shape, and the maximum collapse width is 137 mm. therefore, the length of the first row bolts was set as 16 cm in the following tests.

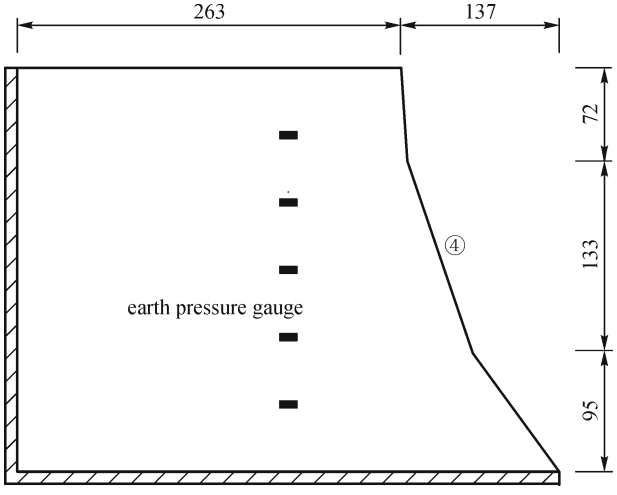

Fig. 12 Final failure face shape of A-A cross-section without bolt reinforcement in case 1 (unit: mm)

Case 2: In this test, there were 5 rows of bolt arranged in the model ground, and each row contains 4 copper tubes with diameter of 1.5mm. As shown in Fig. 13, with the increase of upper load, the cracks ① were also first appeared at the corner of ground surface near side area 2. Subsequently, more cracks, ②, ③ and ④, emerged in ground surface in accordance with the order from the excavation face to far. When the upper load increased further, cracks ⑤ and ⑥ began to appear in the vertical area 2 sequentially. The slope slid to failure eventually when the load increased to 1285 N, and the final sliding face shape is shown in Fig. 14. The bottom of failure face did not pass through the slope foot but appeared at the position just beneath the end of the fifth row bolts. In addition, the maximum collapse width is 118 mm, and the maximum exposed length of the bolt is 106 mm. It shows

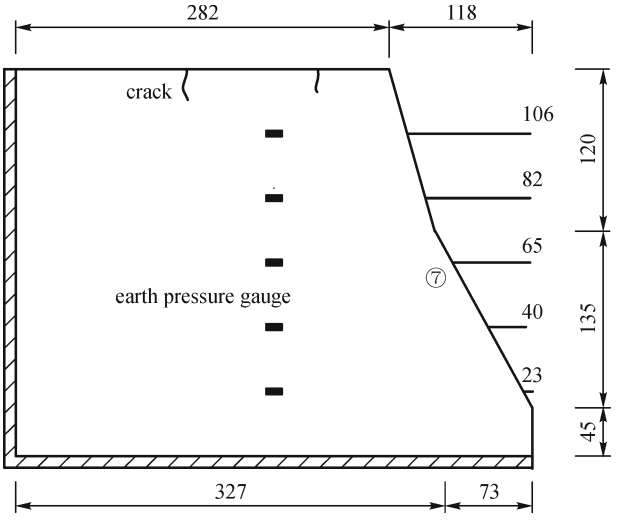

Fig. 14 Final failure face shape of A-A cross-section with bolt reinforcement in case 2 (unit: mm)

that the reinforcement of bolt not only improves the bearing capacity of rock mass, but also makes the collapse range reduced.

Case 3: In this test, there were 5 rows of bolt arranged in the model ground, but each row contains 4 copper tubes with diameter of 1.8mm. With the increase of upper load, the cracks appeared in sequence as the number labeled in Fig. 15. Cracks ① were first appeared at the corner of ground surface near side area 2. Subsequently, cracks ② and ③ emerged in the top of vertical area 2. When the load increased, cracks ④ began to appear in ground surface. With the further increase of upper load, horizontal crack ⑤ appeared at the position of fifth row bolts. As shown in Fig. 16, the final sliding face ⑥ formed when the upper load increased to 1485 N. The bottom of failure face passed through the end of the fifth row bolts. The maximum collapse width is only 73 mm, and the maximum exposed length of the bolt is 60 mm. It seemed that the reinforcement effect in this test is better than that in case 2.

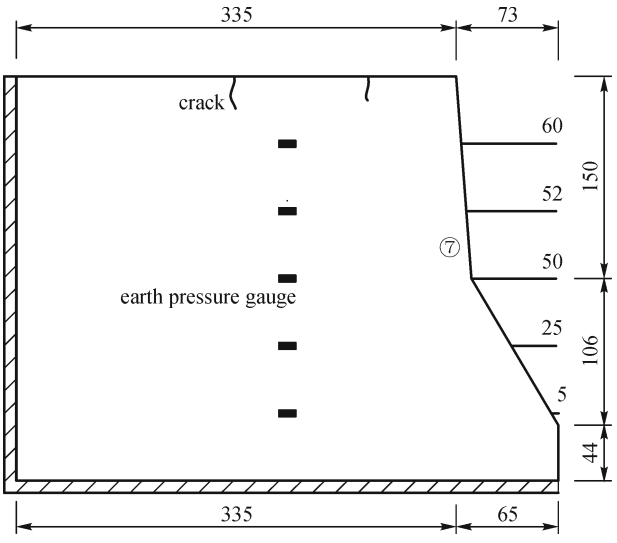

Fig. 16 Final failure shape of A-A cross-section with bolt reinforcement in case 3 (unit: mm)

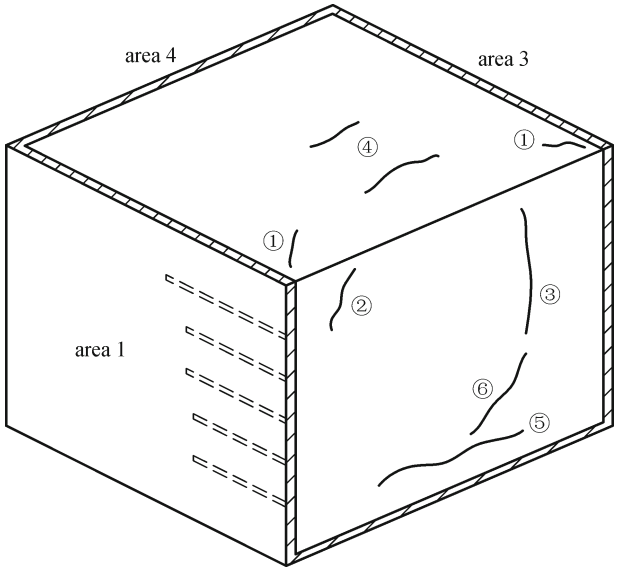

Fig. 15 Progressive failure process of the vertical slope with bolt reinforcement in case 3

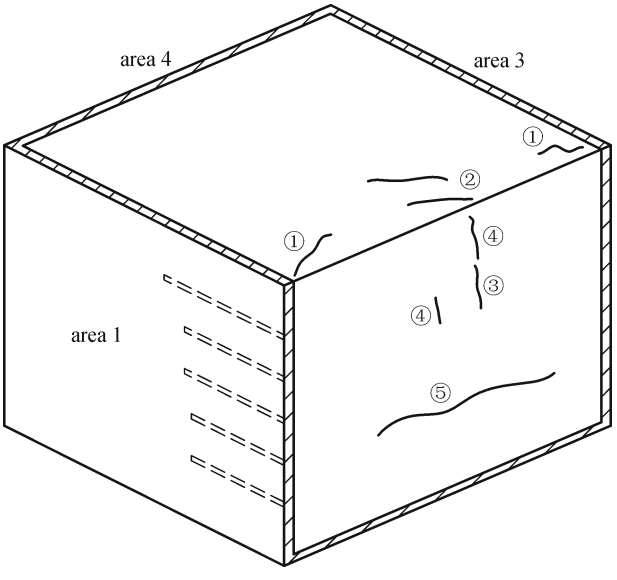

Fig. 17 Progressive failure process of the vertical slope with bolt reinforcement in case 4

Case 4: In this test, there were 5 rows of bolt arranged in the model ground, but each row contains 7 copper tubes with diameter of 1.5 mm. As shown in Fig. 17, crack ① also first started from the corner of ground surface near the vertical area 2. Subsequently, cracks ② appeared at the edge of ground surface. With the further increase of upper load, vertical cracks ③ and ④ emerged from the end of second row bolts to the top of side area 2. After that, horizontal crack ⑤ appeared at the end of fourth row bolts. When upper load increased to 1578 N, the final failure face ⑥ formed. As shown in Fig. 18, the bottom of the final failure face was situated at the end of fourth row bolts. The maximum collapse width is only 50 mm, and the maximum exposed length of the bolt is 40 mm. Obviously, the reinforcement effect in this test was much better than that in case 3.

Case 5: In this test, there were 5 rows of bolt arranged in the model ground, but each row contains 7 copper tubes with diameter of 1.8 mm. As shown in Fig. 19, vertical cracks ①, ② and ③ were first emerged from the end of second row bolts to the top of side area 2. With the increase of upper load, cracks ④ began to appear at the corner of ground surface edge. When the upper load increased further, crack ⑥ appeared in the middle of ground surface, and crack ⑤ in side area 2 extended to horizontal crack ⑦. After that, local area ⑧ collapsed at the slope foot, and horizontal crack ⑨ appeared at the end of the fifth row

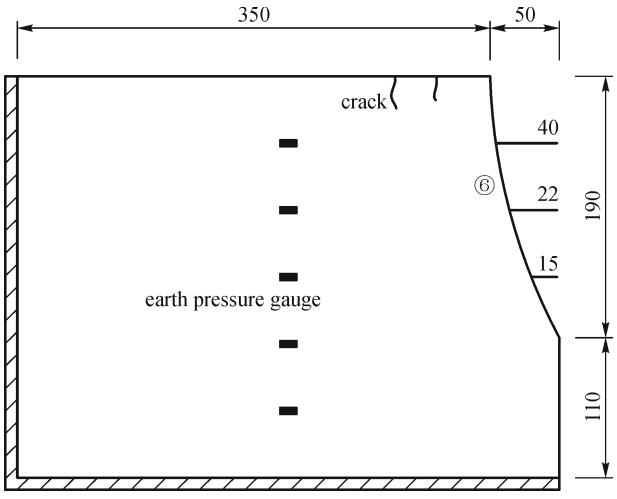

Fig. 18 Final failure shape of A-A cross-section with bolt reinforcement in case 4 (unit: mm)

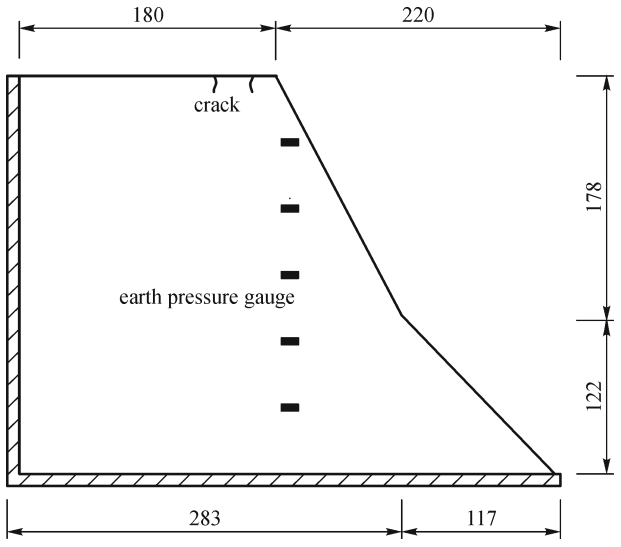

Fig. 20 Final failure shape of A-A cross-section with bolt reinforcement in case 5 (unit: mm)

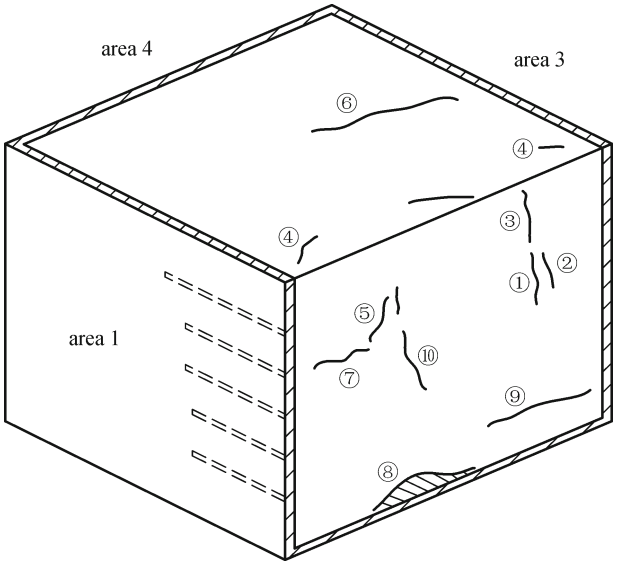

Fig. 19 Progressive failure process of the vertical slope with bolt reinforcement in case 5

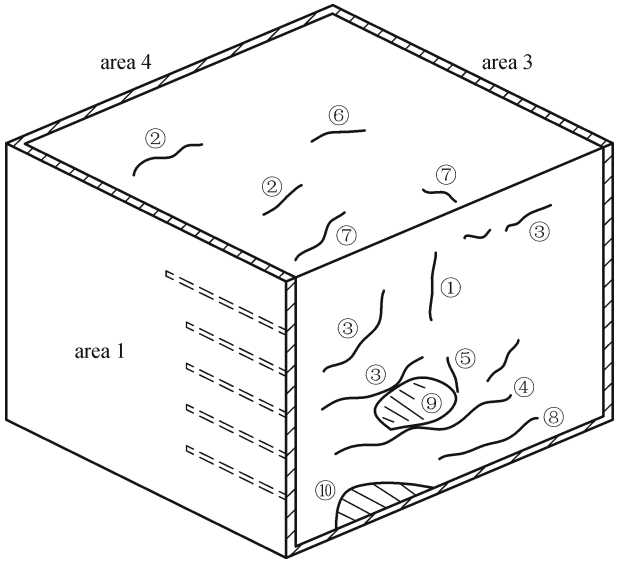

Fig. 21 Progressive failure process of the vertical slope with bolt reinforcement in case 6

bolts. When the upper load increased again, vertical crack ⑤ extend downwards to crack ⑩. Once the load exceeded 1629 N, the failure face slid behind the inner end of the bolts, as shown in Fig. 20.

Case 6: In this test, there were 5 rows bolts arranged in the model ground, but each row contains 6 copper tubes with diameter of 2.0 mm. Crack ① first appeared at the top of side area 2, as shown in Fig. 21. Subsequently, cracks ② emerged in the middle of ground surface. With the increase of upper load, some horizontal and oblique cracks ③ appeared at the upside of side area 2, especially at the position between the second and the third row bolts. After that, horizontal cracks ④ and ⑤ emerged at the third and the fourth row bolts in side area 2. When the upper load increased again, cracks ⑥ and ⑦ appeared in the ground surface, and then horizontal crack ⑧ appeared at the end of fifth row bolts. When the upper load increased to a certain value of 1655 N, local range ⑨ and ⑩ collapsed in sequence, and the final failure face shape is shown in Fig. 22.

Case 7: In this test, there were 5 rows of bolt arranged in the model ground, but each row contains 6 copper tubes with diameter of 2.0 mm. As shown in Fig. 23, first, vertical cracks ① appeared at the upside of side area 2, then it extended downwards to horizontal cracks ②. Due to the increase of upper load, oblique crack ③ emerged at

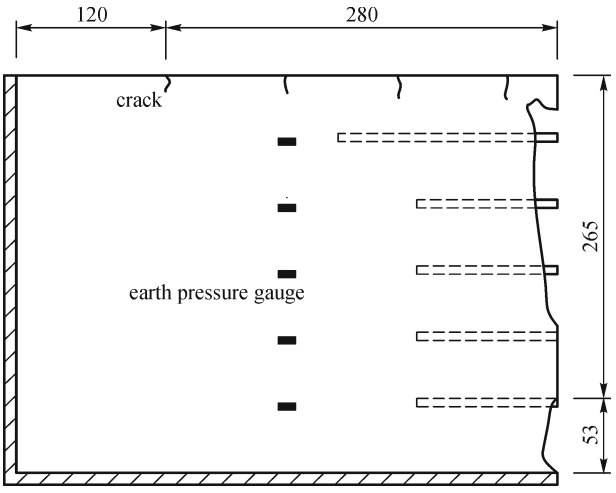

Fig. 22 Final failure shape of A-A cross-section with bolt reinforcement in case 6 (unit: mm)

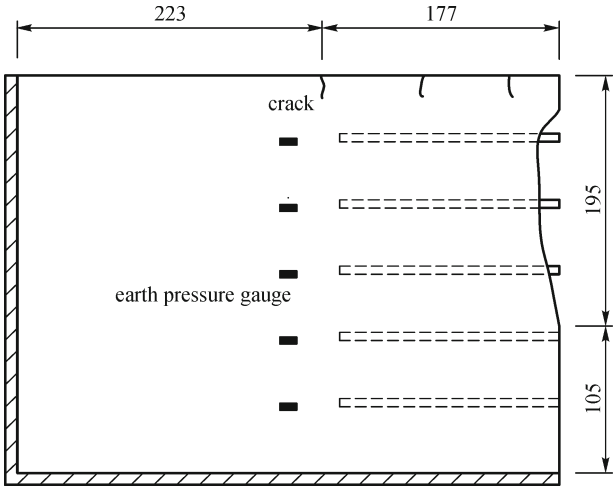

Fig. 24 Final failure shape of A-A cross-section with bolt reinforcement in case 7 (unit: mm)

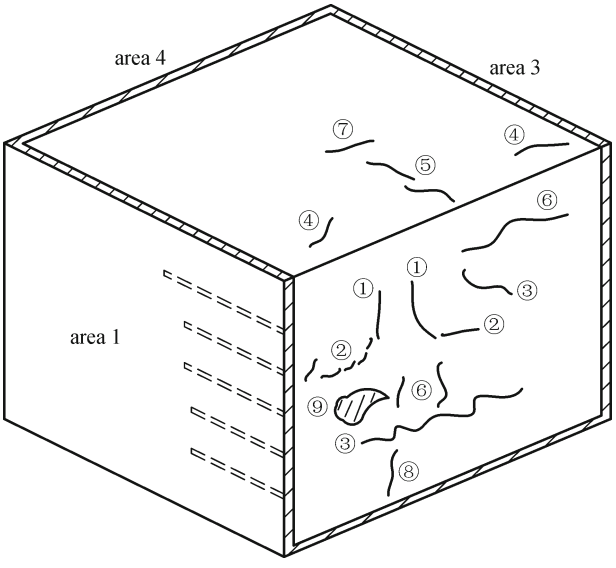

Fig. 23 Progressive failure process of the vertical slope with bolt reinforcement in case 7

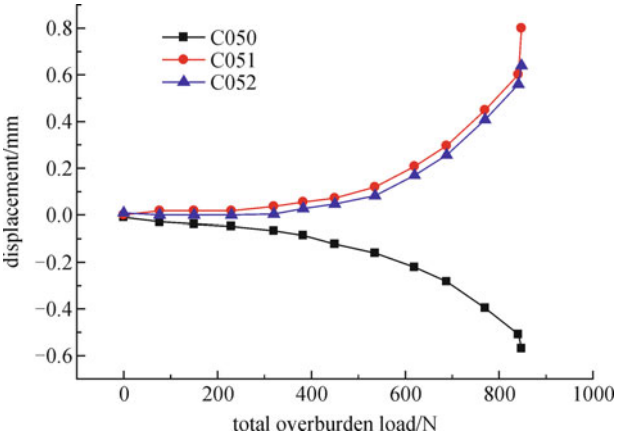

Fig. 25 Variation of displacement curve in case 1

the end of second row bolts, and horizontal crack ③ at the end of fourth row bolts. Subsequently, cracks ④ appeared at the corner and ⑤ in the middle of ground surface edge. When upper load increased again, more cracks ⑥ emerged in the side area 2, and crack ⑦ in the middle of ground surface. After that, vertical crack ⑧ formed at the slope bottom, and the local range ⑨ collapsed at the end of third row bolts. The final failure shape is shown in Fig. 24.

5.2 Displacement results analysis

Case 1: As shown in Fig. 25, the ground surface displacement measuring point of C050 assumed declined trend. The other two points measuring the horizontal displacement of side wall, C051 and C052, continued to rise with the increase of upper load. Before the load reached 300 N, the displacement of each point was not very obviously. But once the load exceeded 500 N, the displacement of each point presented acceleration trend. When the load reached 848 N, there was a drastic change in the displacement, which corresponding to the failure of the slope. In addition, the displacement of point C051 close to ground surface was higher than that of C052. Before the slope collapse, the maximal displacement of side wall is 0.64 mm, and that of ground surface is 0.51 mm.

Case 2: As seen from Fig. 26, the rock deformation increased obviously when the overburden load reached 400 N; after 900 N, it increased more quickly. Finally, the slope failed at 1285 N. Before the slope collapse, the maximal displacement of side wall was 1.26 mm, and that of ground surface is 0.46 mm. We can see that, due to the anchoring effect of bolt, the rock slope bearing capacity increased from 848 N to 1285 N. Additionally, the rock

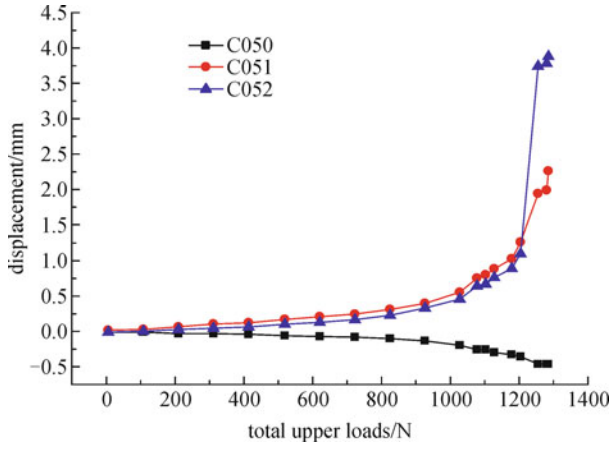

Fig. 26 Variation of displacement curve in case 2

deformation value of side wall in this test was higher than that in case 1, correspondingly, the ground surface displacement was lower than that in case 1.

Case 3: As shown in Fig. 27, the displacement of C051 close to ground surface began to vary obviously when the overburden load increased to 500 N; but C050 and C052 did not increase obviously until 800N. When the upper load reached 1200 N, the displacement of all measuring points increased rapidly. The slope collapsed finally at the load of 1485 N. As compared with case 2, the copper pipe diameter increased from 1.5 mm to current 1.8 mm, accordingly, the rock bearing capacity increased from 1285 N to 1485 N. Additionally, before the slope collapse, the maximal displacement of side wall was 1.32 mm, and the ground surface was only 0.17 mm.

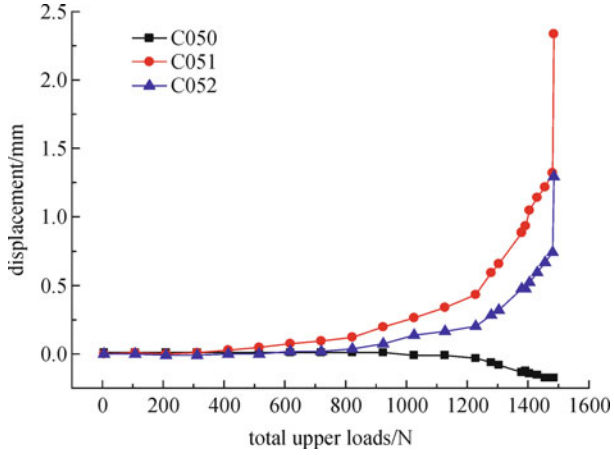

Fig. 27 Variation of displacement curve in case 3

Case 4: Since the fault of C052, its result was not reflected in Fig. 28. We can see that, the deformation began to vary obviously when the upper load increased to 600 N. Once the load reached 1200 N, the displacement of both the ground surface and the side wall increased rapidly until

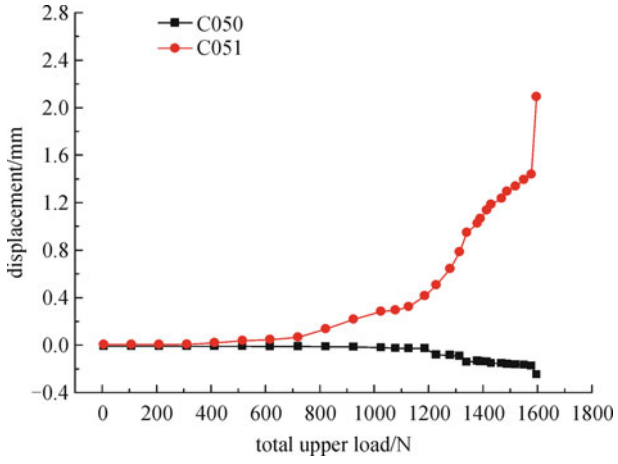

Fig. 28 Variation of displacement curve in case 4

the slope collapsed at 1578 N. Before the slope collapse, the maximal displacement of side wall was 1.43 mm, and the ground surface was 0.18 mm.

Case 5: As shown in Fig. 29, the deformation also varied obviously when the upper load is 700 N. After the load reached to 1100 N, the deformation rate increased again, but its growth rate slowed down when the load exceeded 1500 N. The slope finally collapsed at the load of 1629 N, and the failure load was a little higher than that in case 4. Before the slope collapse, the maximal displacement of side wall was 2.2 mm, and the ground surface was 0.54 mm.

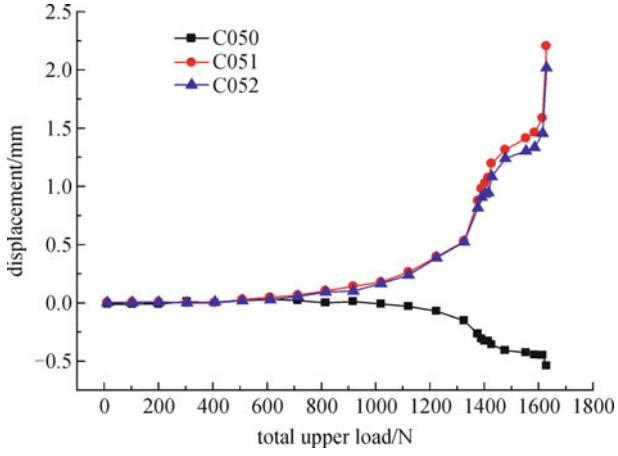

Fig. 29 Variation of displacement curve in case 5

Case 6: It can be seen from Fig. 30 that, the rock deformation varied obviously at the load of 800 N, and increased rapidly when the load reached 1000 N. From then on, the deformation rate of C052 kept relatively stable. When the overburden load increased to 1655 N, the side wall suddenly collapsed. At this time, the maximal displacement of side wall was 1.76 mm, and the ground surface was 0.57 mm.

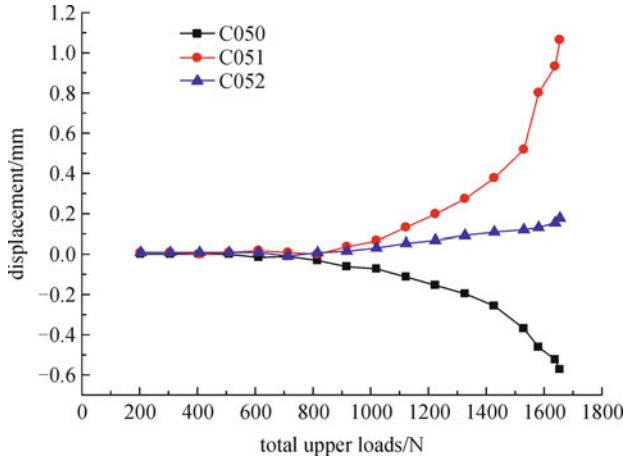

Fig. 30 Variation of displacement curve in case 6

Case 7: As shown in Fig. 31, the deformation varied obviously started from 800 N. When the overburden load was 1200 N, the side wall deformed outwards quickly, and the ground surface settled rapidly after 1200 N. The side wall collapsed when the load exceeded 1713 N. At his time, the maximal displacement of side wall was 1.76 mm, and the ground surface was 0.28 mm.

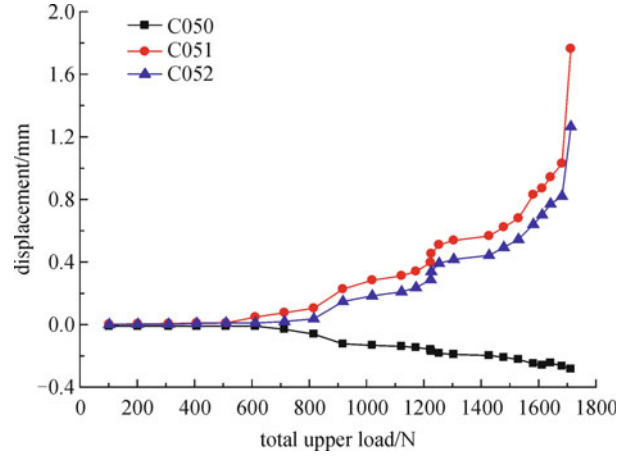

Fig. 31 Variation of displacement curve in case 7

5.3 Stress variation value results analysis

Case 1: Figs. 32 and 33 show the variation history of horizontal stress inside rock mass in case 1. We can see that, first, the rock stress began to vary obviously when the overburden load increased to 300 N. Secondly, with the increase of overburden load, the horizontal stress at −50 mm position kept growing until the load of 450 N; the other four measured horizontal stress continued to grow before the slope collapsed at 840 N, after that, it declined rapidly. It means the topside of rock slope is often prone to tensile failure; therefore, cracks were first generated in the shallow layer near ground surface.

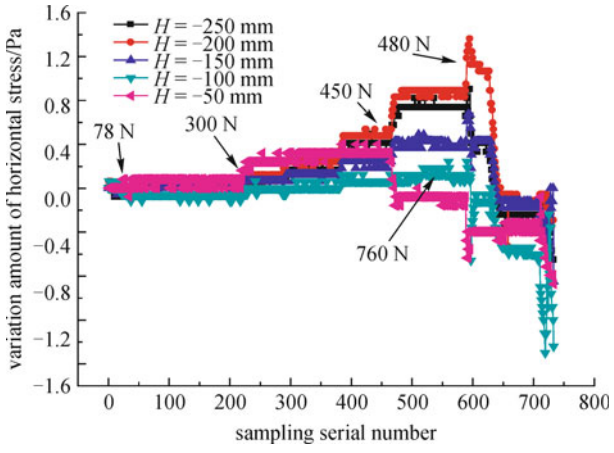

Fig. 32 Variation of horizontal stress during the loading process without bolt reinforcement in case 1

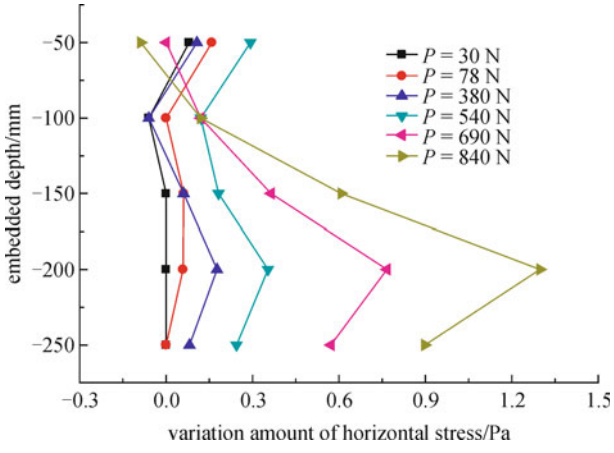

Fig. 33 Variation of horizontal stress at different depth without bolt reinforcement in case 1

Thirdly, from the ground surface down to the inner side of rock mass, the stress increment at −200 mm position is maximal, which means that the rock mass here is vulnerable to compression and shear destruction. That is to say, the failure at the slope bottom always starts from the inner side of rock mass, not from the rock surface.

Figures 34 and 35 present the variation history of vertical stress inside the rock mass. As can be seen, the vertical stress also varied obviously from 300 N. With the increase of overburden load, except for the vertical stress at −50 mm kept declining, the other four measured vertical stress continued to grow before the slope collapsed at 840N. Additionally, the stress increment at −100 mm position is maximal, which means that the rock mass here is also vulnerable to destroy. Furthermore, from Fig. 35 we can see that, when the load exceeded 840 N, the position of maximal vertical stress moved from −100 mm to −150 mm. That means the slide face began to develop from the top to the bottom of slope.

Case 2: The variation histories of horizontal stress inside

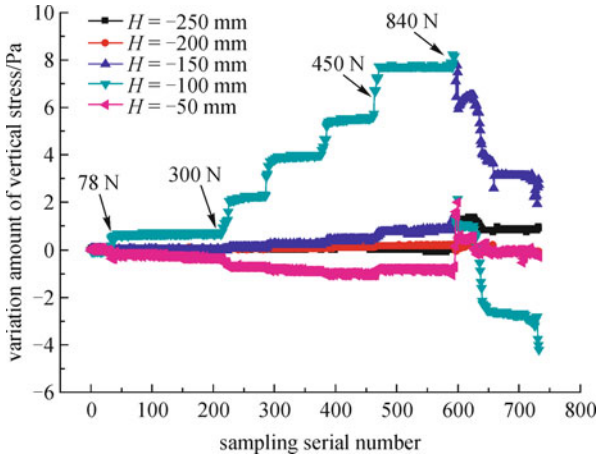

Fig. 34 Variation of vertical stress during the loading process without bolt reinforcement in case 1

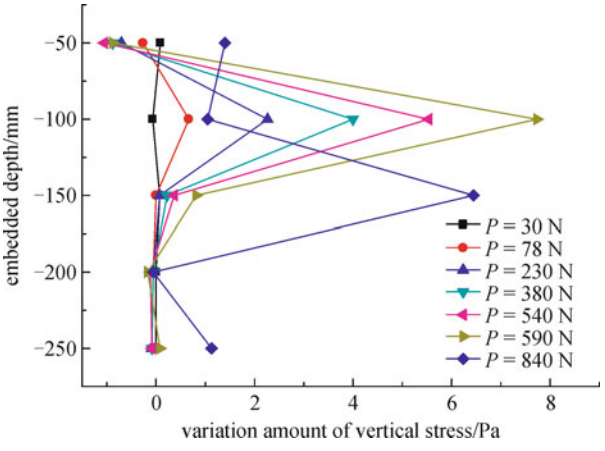

Fig. 35 Variation of vertical stress at different depth without bolt reinforcement in case 1

rock mass in case 2 are shown in Figs. 36 and 37. The

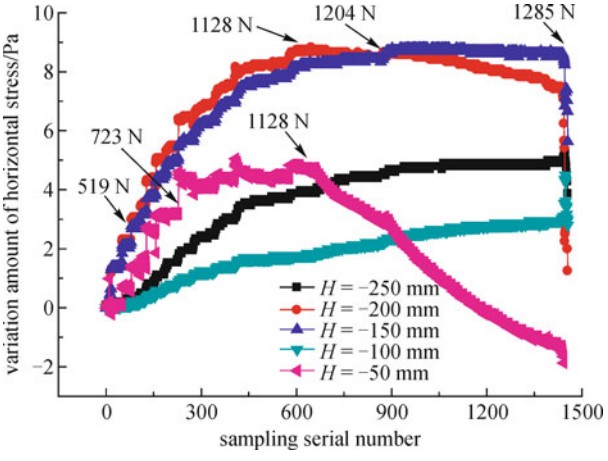

Fig. 36 Variation of horizontal stress during the loading process with bolt reinforcement in case 2

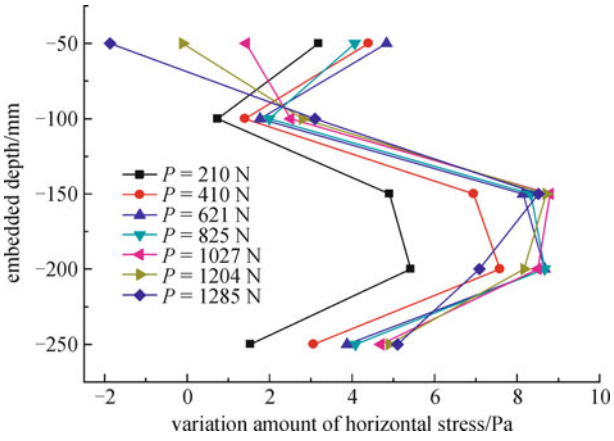

Fig. 37 Variation of horizontal stress at different depth with bolt reinforcement in case 2

stress at −50 mm position grew with the increase of the overburden load until 1128 N, and it then declined gradually. That means the rock slope also destroyed from the top side first though it had been reinforced with bolt. During the whole test process, the stress increment at −150 mm and −200 mm position were relatively large, and the stress at −150 mm was higher after 1204 N. It means that, due to the effect of bolt reinforcement, the stress concentration was dispersed in some degree.

Figures 38 and 39 show the variation histories of vertical stress inside the rock. Its variation law is a little similar with that in case 1. The stress at −50 mm position decreased quickly at 312 N, and the stress at −100 mm always kept maximal. The difference is that the stress at −150 mm is also very high and close to that at −100 mm.

Case 3: As seen from Figs. 40 and 41, the most significant feature is that the horizontal stress increment at −50 mm position dropped quickly at 510 N and entered stable stage at the overburden load of 1025 N. The stress variation amount at −100 mm is also smaller and began to

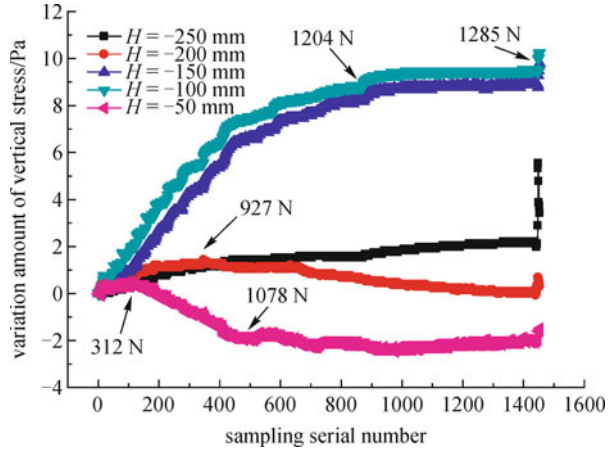

Fig. 38 Variation of vertical stress during the loading process with bolt reinforcement in case 2

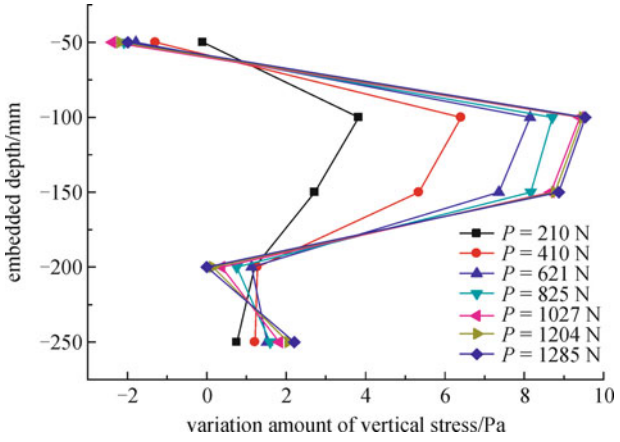

Fig. 39 Variation of vertical stress at different depth with bolt reinforcement in case 2

decrease at 1228 N. Furthermore, the stress increment at −200 mm position is relative smaller than that in case 2. That means the high compressive shear effect in the rock mass at slope bottom is further alleviated.

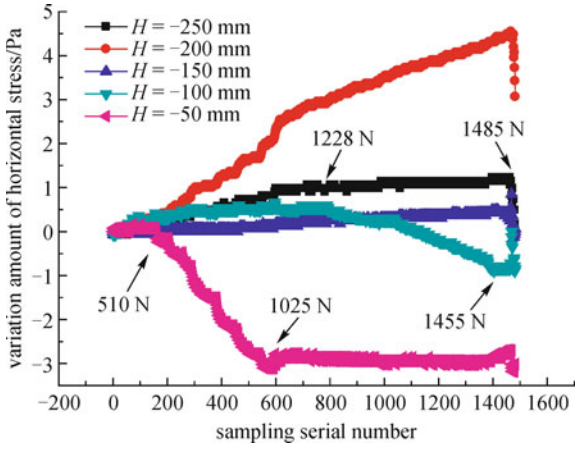

Fig. 40 Variation of horizontal stress during the loading process with bolt reinforcement in case 3

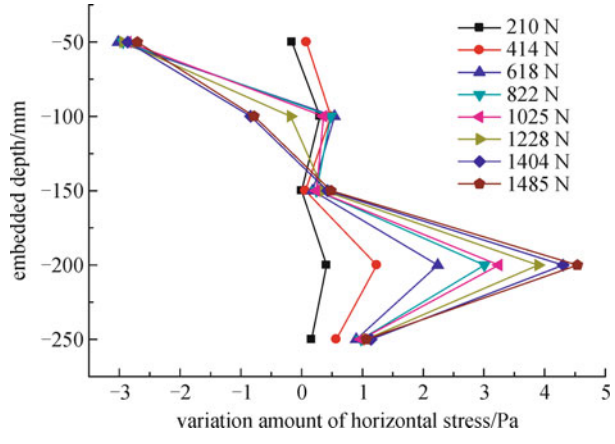

Fig. 41 Variation of horizontal stress at different depth with bolt reinforcement in case 3

From Figs. 42 and 43 we can see that, all the vertical stress increments present the trend of growing first, and then declined in accordance with the order from top to bottom in sequence of upper load at 715 N, 1025 N, 1330 N, 1455 N and 1485 N. In addition, the maximal vertical stress increment presents the trend of growing gradually with its position moving from −100 mm downwards. That means, due to bolt reinforcement, the slope is not easy to be damaged at the bottom, but the rock failure often develops from top to bottom.

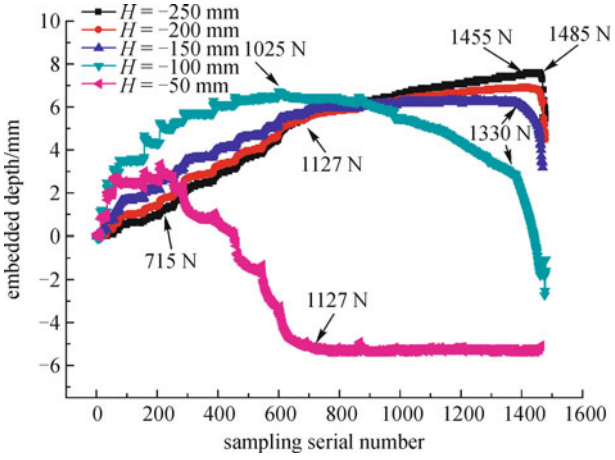

Fig. 42 Variation of vertical stress during the loading process with bolt reinforcement in case 3

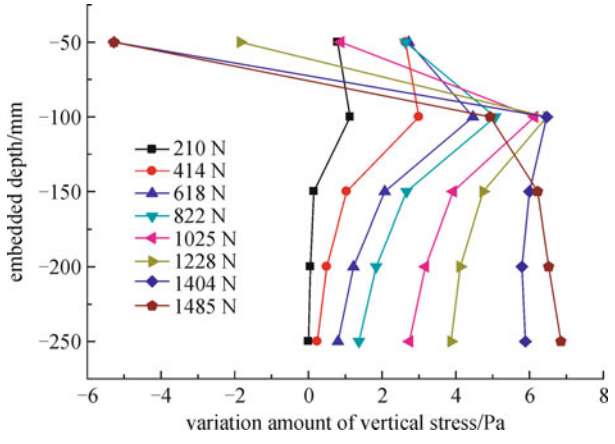

Fig. 43 Variation of vertical stress at different depth with bolt reinforcement in case 3

Case 4: The variation values of horizontal stress are shown in Figs. 44 and 45. With the increase of upper loads, the stress at −50 mm presents decreasing trend, and the stress at −100 mm varies slightly. The other three stress values below −100 mm increase rapidly until 816 N, and then entered a relatively stable state, in which, the stress increment value at −250 mm position is the largest.

In Figs. 46 and 47, the variation law of vertical stress is some what similar with that in case 3. It should be pointed

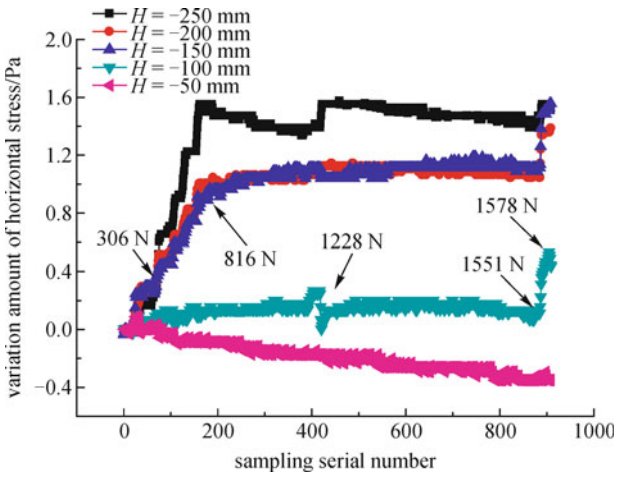

Fig. 44 Variation of horizontal stress during the loading process with bolt reinforcement in case 4

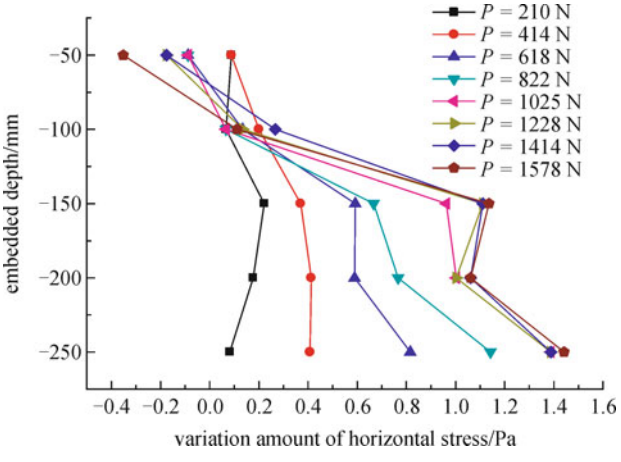

Fig. 45 Variation of horizontal stress at different depth with bolt reinforcement in case 4

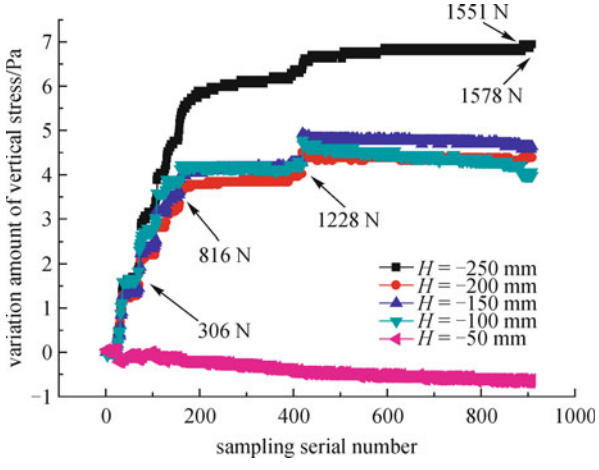

Fig. 46 Variation of vertical stress during the loading process with bolt reinforcement in case 4

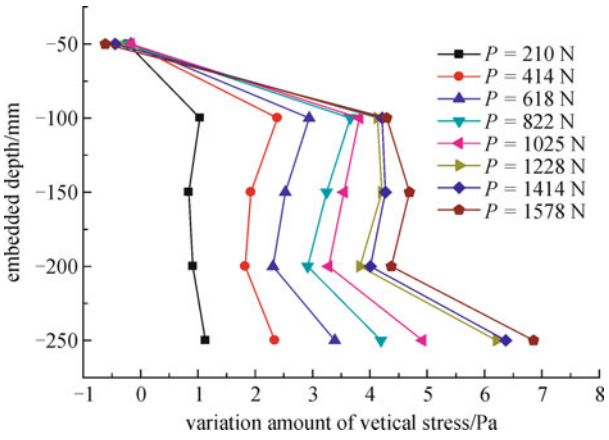

Fig. 47 Variation of vertical stress at different depth with bolt reinforcement in case 4

out that the stress variation at −50 mm is very small, though it mainly declined during the whole test process. The other three stress increment grew rapidly before 1228 N and then kept in relatively state until the slope collapses.

Case 5: As seen from Figs. 48 and 49, the stress at −50 mm decreased gradually until 1020 N, and then in a relatively stable state. Secondly, the stress at −100 mm grew first and then declined from the load value of 1402 N. Thirdly, at the location of −150 mm, the stress varies very slightly.

According to Figs. 50 and 51, all the stress rose first and then descended gradually. Another feature is that the location of maximal stress increment gradually moving from −100 mm down to −150 mm.

Case 6: As seen from Figs. 52 and 53, the most significant feature of the horizontal stress is that, the stress at −100 mm rose steeply and then decreased rapidly, and

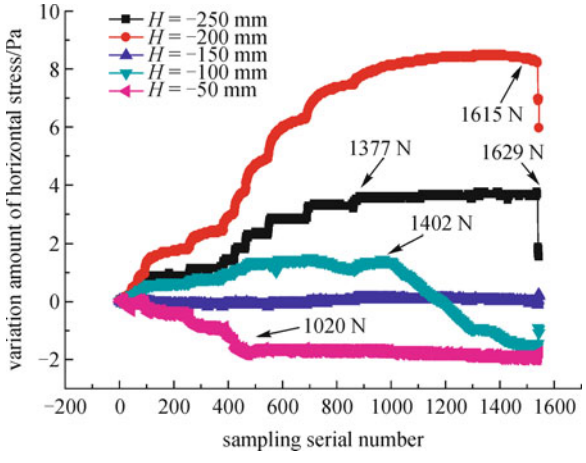

Fig. 48 Variation of horizontal stress during the loading process with bolt reinforcement in case 5

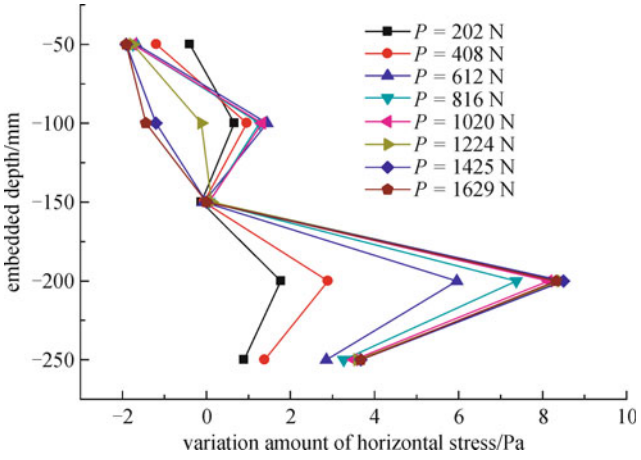

Fig. 49 Variation of horizontal stress at different depth with bolt reinforcement in case 5

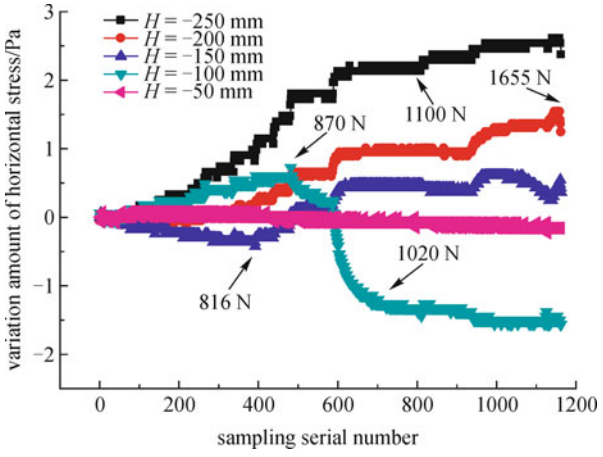

Fig. 52 Variation of horizontal stress during the loading process with bolt reinforcement in case 6

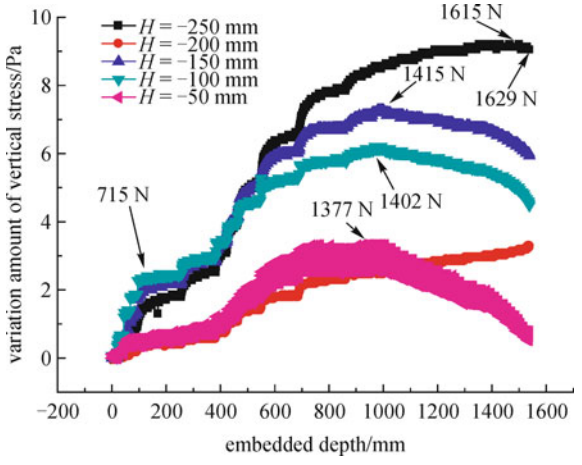

Fig. 50 Variation of vertical stress during the loading process with bolt reinforcement in case 5

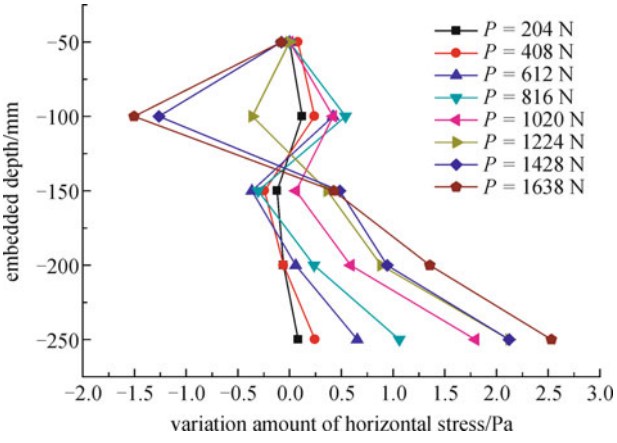

Fig. 53 Variation of horizontal stress at different depth with bolt reinforcement in case 6

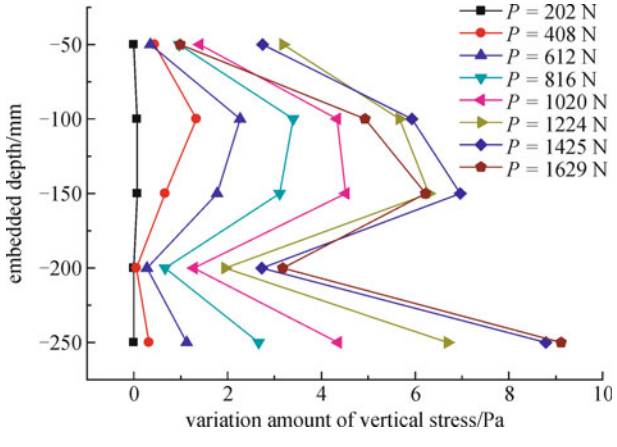

Fig. 51 Variation of vertical stress at different depth with bolt reinforcement in case 5

the stress at −150 mm decreased first, and then rose gradually.

The variation values of vertical stress are shown in Figs. 53 and 54. The vertical stress at −50 mm increased slowly until the upper load of 715 N, and then decreased gradually. The stress value at −100 mm position began to decrease at the load of 918 N. In addition, during the whole test process, the stress increment at −150 mm position is maximal.

Case 7: As shown in Figs. 56 and 57, the stresses at the position of −50 mm, −200 mm, −250 mm increased slightly, and then kept relatively stable. The stresses at −100 mm and −150 mm decreased first and then enter stable state at 1220 N and 1370 N respectively.

From Figs. 58 and 59, we can see that, the other four stress grew gradually, except that the stress at −50 mm rose quickly and then decreased rapidly. The stress at −100 mm always kept maximal, it began to deceased at 1422 N.

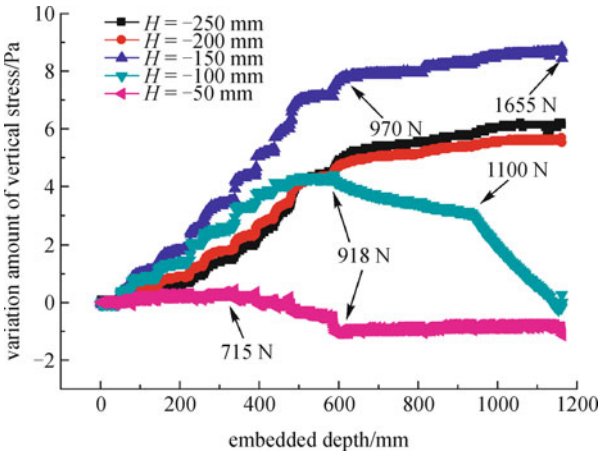

Fig. 54 Variation of vertical stress during the loading process with bolt reinforcement in case 6

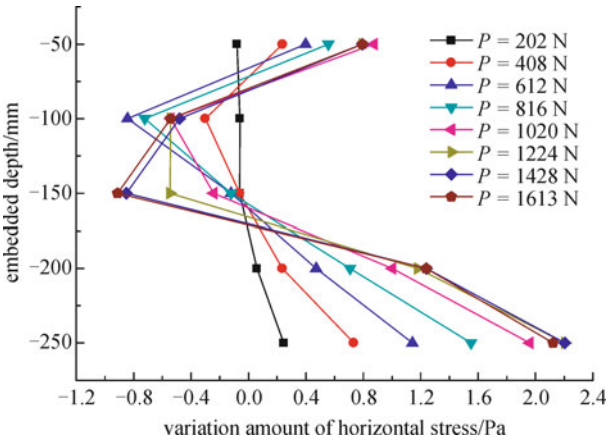

Fig. 57 Variation of horizontal stress at different depth with bolt reinforcement in case 7

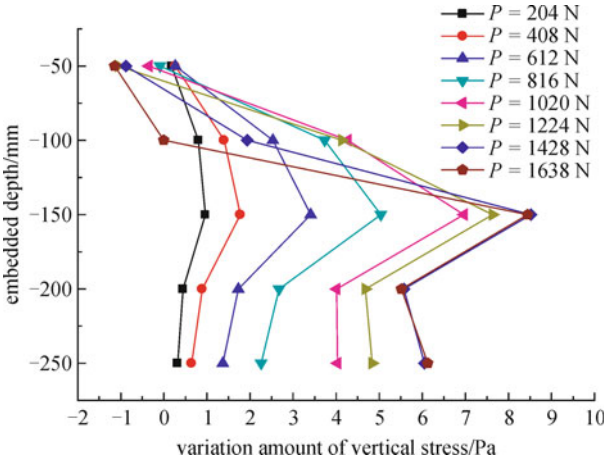

Fig. 55 Variation of vertical stress at different depth with bolt reinforcement in case 6

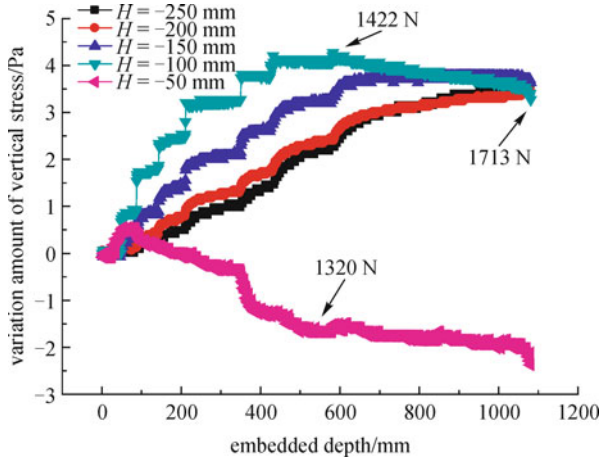

Fig. 58 Variation of vertical stress during the loading process with bolt reinforcement in case 7

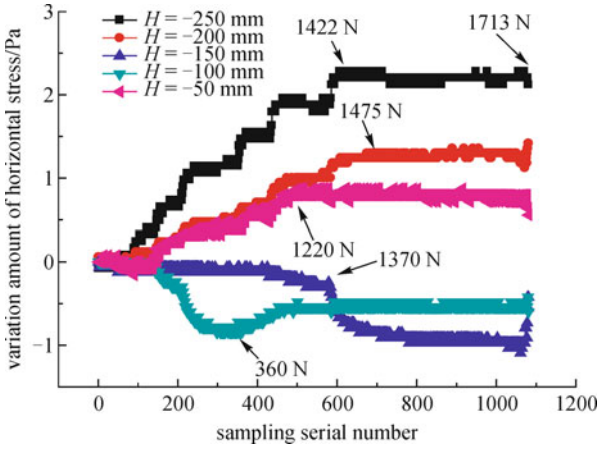

Fig. 56 Variation of horizontal stress during the loading process with bolt reinforcement in case 7

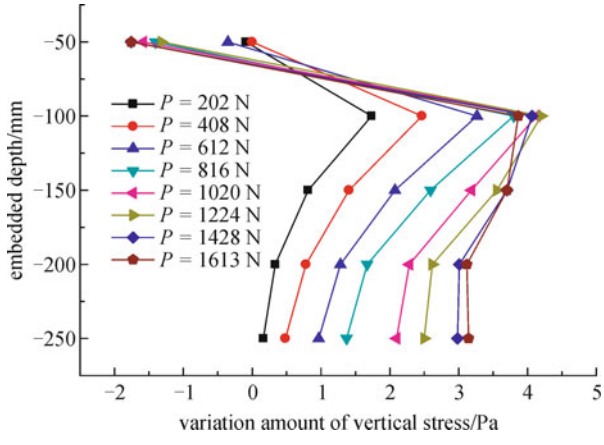

Fig. 59 Variation of vertical stress at different depth with bolt reinforcement in case 7

6 Conclusions

To improve the understanding on the failure behavior and its anchoring effect of weak-broken rock slope, the rock of grade IV according to China is taken as reference object, and a series of model tests were carried out in laboratory. Based on the analysis of test results, some conclusions can be drawn:

1) As for weak-broken rock slope, it is the combined results of tension-shear failure in the shallow ground and the compression-shear failure in the deep rock mass near slope bottom. Mostly, the rock slope failure starts first from the top ground surface, and the failure presents progressive mechanism.

2) The findings on the fractures emergency sequence and its development law in the rock slope surface do good to improve the understanding of failure behavior of prototype weak-broken rock slope.

3) The anchoring effect of bolt was reflected by the aspects of shear resistance, crack resistance and anti-extension. More importantly, due to reinforcement of bolt, the stress concentration in rock mass is alleviated, which do reduce the self-risk of rock damage.

4) If the slope was anchored with bolt, it not only can reduce vertical subsidence of rock slope but also allow larger horizontal deformation of side wall before the slope collapses eventually.

5) During the progressive process of slope, if no bolt reinforced, the horizontal stress increment decreased in the shallow rock mass, but increased greatly in the deep inner side just above slope foot. On the other hand, the maximal vertical stress increment mainly located in the shallow rock mass just beneath ground surface, but it moved downwards before the slope collapses eventually.

6) If the slope was reinforced with bolt, the horizontal stress in the shallow would also decrease drastically, and this decline trend moved downwards with the increase of upper load. At the slope bottom, the horizontal stress rise obviously, especially in the deepest. On the other hand, with the increase of upper load, except that the vertical stress in the shallow rock mass decreased gradually, the other stresses from top to down increased gradually and tended to be the same value.

7) Reasonable bolt diameter and anchoring space has important influence on the stability of rock slope, and reasonable bolt length can more effectively improve the safety and stability of rock slope.

Acknowledgements This research work is supported by the National Natural Science Foundation of China (Grant No. 40672184) and the Open Foundation of the Key Laboratory of Geotechnical and Underground Engineering of Ministry of Education of China.

References

1. Zhang P, Li N, He L R. Research on localized progressive damage model for fractured rocklike materials. Chinese Journal of Rock Mechanics and Engineering, 2006, 25(10): 2043–2050 (in Chinese)
2. Hatzora Y H, Arzib A A, Zaslavsky Y, et al. Dynamic stability analysis of jointed rock slopes using the DDA method: King Herod's Palace, Masada, Israel. International Journal of Rock Mechanics and Mining Sciences, 2004, 41(5): 813–832
3. Sterpi D, Cividini A. A Physical and numerical investigation on the stability of shallow tunnels in strain softening media. Rock Mechanics and Rock Engineering, 2004, 37(4): 277–298
4. Eberhardta E, Steadb D, Cogganc J S. Numerical analysis of initiation and progressive failure in natural rock slopes-the 1991 Randa rockslide. International Journal of Rock Mechanics and Mining Sciences, 2004, 41(1): 69–87
5. Crook T, Willson S, Yu J G, et al. Computational modelling of the localized deformation associated with borehole breakout in quasi-brittle materials. Journal of Petroleum Science Engineering, 2003, 38(3): 177–186
6. Fan W, Yu M H, Shi Y W, et al. The unified solution of the plastic relaxed pressure s computing of surrounding rock masses. Journal of Xian Engineering University, 2003, 25(1): 33–36 (in Chinese)
7. Liu Y G, Zhou W Y, Zhao J D, et al. Discontinuous bifurcation model of damage localization for jointed rocks and its application. Acta Mechanica Sinica, 2003, 35(4): 411–418 (in Chinese)
8. Zheng Y R, Zhao S Y, Deng W D. Numerical simulation on failure mechanism of rock slope by strength reduction FEM. Chinese Journal of Rock Mechanics and Engineering, 2003, 22(12): 1943–195 (in Chinese)
9. Wang G S. The progressive failure of slope and the stability analyses. Chinese Journal of Rock Mechanics and Engineering, 2000, 19(1): 29–33 (in Chinese)
10. Cheng Q G, Hu H T, Peng J B, et al. Visco-elastoplastic finite element simulation of progressive failure of high-steep rock slope. Journal of Engineering Geology, 2000, 8(1): 25–30 (in Chinese)
11. Li X. Finite element analysis of slope stability using a nonlinear failure criterion. Computers and Geotechnics, 2007, 34(3): 127–136
12. Yuan D X, Zhu Z L, Zhu Q S. Experimental research on geomechanics model of jointed rock mass of high slope. Journal of China Three Gorges University, 2001, 23(3): 193–197 (in Chinese)
13. Wu D H, Zeng X Y, Dun A F, et al. Experimental study on rock model of cracked structure reinforced by single bolt. Underground Space, 2003, 23(2): 158–161 (in Chinese)
14. Chen Y J, Wang J C, Chang L S, et al. Experimental research on progressive failure of jointed rock slope. Underground Space, 2003, 23(2): 158–161 (in Chinese)
15. Liu X Q, Zhu J M, Feng J Y, et al. Mechanism of the slope failure of horizontal thick coal seam under the condition of combined mining. Journal of China Coal Society, 2008, 33(12): 1346–1350 (in Chinese)